Electron-positron annihilation characteristics at a metal surface: simple metals

1993 J. Phys.: Condens. Matter 5 8195

(http://iopscience.iop.org/0953-8984/5/44/011)

J. Phys.: Condens. Matter 5 (1993) 8195–8210. Printed in the UK

Electron–positron annihilation characteristics at a metal surface: simple metals

A Rubaszek†, A Kiejna‡ and S Daniuk§

† W Trzebiatowski Institute of Low Temperature and Structure Research, Polish Academy of Sciences, 50-950 Wrocław 2, PO Box 937, Poland

‡ Institute of Experimental Physics, University of Wrocław, 50-204 Wrocław, Pl. Maxa Borna 9, Poland

§ Dachblach, 52-429 Wrocław, Morelowskiego 105, Poland

Received 27 July 1993

Abstract. Momentum densities of annihilating electron–positron pairs, positron lifetimes, work functions and binding energies as well as electron–positron enhancement factors at the surfaces of simple metals and cadmium are studied. The effect of electron–positron correlations on the surface-state positron annihilation characteristics is set out.

1. Introduction

Studies of slow positron interactions with metal surfaces (for reviews, see e.g. [1]–[4]) opened a new channel in investigations of the electronic structure of solids by positron annihilation. In particular, the extended well known angular correlation of annihilation radiation (ACAR) technique (for reviews, see e.g. [5,6]) has been successfully applied to probing electron and positron surface states (SS) in Al ([7–10]), Cu [11], Ni [9, 10, 12], Pb [13], Si [9, 10] and graphite [14].

Slow-positron experiments have confirmed the presence of the positron SS at the clean Al [110] surface [15]; the SS component of the measured lifetime spectrum amounts to 580 ps, i.e. about 15% more than the spin-averaged free positronium value. This result is surprising from the point of view of positron annihilation characteristics in bulk matter. Furthermore, unlike the ACAR spectra from the Cu, Ni and Pb surfaces [9–14], which display strong anisotropy (in agreement with theoretical expectations), the SS components of the two-dimensional (2D) ACAR spectra from any of three low-index surfaces of Al ((100), (110) and (111)) are nearly isotropic and face independent [9, 10]. The question is how far these unexpected features of the SS annihilation characteristics in Al may be attributed to the nearly free character of valence electrons in the bulk aluminium? A clear answer would give the positron annihilation parameters at the surfaces of other simple metals, characterized by nearly parabolic valence bands in the bulk. The experiment on clean surfaces of simple metals is, however, very difficult to perform; these metals are very active and the oxidation layer is created at the surface within a few minutes, changing the properties of the material (e.g. electron and positron work functions) appreciably. Thus, if an ultra-high vacuum is not available, the positron SS may not even be observed [16].

In theoretical studies of the lifetime and ACAR spectra of a positron trapped at a metal surface, various effects should be taken into account. First, the knowledge of distributions of individual electronic states in the host material is of vital importance, at least for the region

0953-8984/93/448195+16$07.50

where the positron is found with high probability [17]. For this reason the mixed density approximation [18] should be abandoned in calculations of ACAR spectra at the surface, as noted in [20]. Electron–positron correlations must be treated very carefully in the near-surface region. If the enhancement of electron density on the positron is neglected (see [18, 19, 21–23]), the SS lifetime is one order of magnitude longer than the experimental one. The local density approach (LDA) to electron–positron correlations leads to underestimation of the SS lifetime at the Al surface [18, 19] and to too narrow ACAR spectra [24]. Moreover, the expected image form of the electron–positron correlation potential far outside the surface plane is never reproduced within LDA. Application of the weighted-density approximation (WDA) (introduced by Gunnarson *et al* [25]) allows the avoidance of these deficiencies of LDA and provides the correct theoretical value of the lifetime for a positron trapped at the Al surface [17, 26]. Finally, the shape of the positron wave function, which depends on both the unperturbed electron density distribution in the material and electron–positron correlation effects, has a crucial influence on the resulting annihilation characteristics (cf [27–29]). All the problems at issue should be treated on a broad basis in a consistent way when the annihilation parameters for positrons trapped at the metal surface are investigated.

Simple metals seem to be most convenient for studies of the influence of various effects on the SS annihilation characteristics. The jellium-like character of valence electrons well inside these metals (see [30]), and therefore in the planes parallel to the surface, allows us to evade complicated band-structure calculations at the surface, which are necessary in the case of the d-electron metals (in both cases the core-electron contribution to the SS annihilation characteristics is almost negligible because the probability that the rare-gas core electrons escape from the metal to vacuum is very low). As a consequence, one avoids possible imperfections of the standard band-structure methods adapted to the surface problem, which can occur if the fact that the periodicity conditions are violated normal to the surface plane is not taken exactly into account in the formalism. Moreover, in contrast to the transition metals, for which the correlation effects should be considered separately for d- and sp-type electronic populations (cf [29, 31, 32]), in simple metals we are able to get rid of difficulties connected with determining energy dependence of electron–positron enhancement factors at the surface (e.g. if the approximation developed in [17] is used).

In the present work an approach proposed in [20] and [17] is applied to calculations of the SS ACAR spectra, lifetimes and enhancement factors from the surfaces of Al, Cd, Mg, Li, Na and K. Electron wave functions in the host material are determined in the way developed by Kiejna [33]. Electron–positron correlations are included to the formalism within WDA. In the positron model the energy levels in the bulk, following from the linear-muffin-tin orbital (LMTO) average-spheres approximation (ASA) results of [29], are taken into account providing positron work functions and binding energies.

2. Formalism

The positron partial and total annihilation rates are given by the expressions (see, e.g. [6, 34–36])

$$\rho(p) = \frac{\pi r_0^2 c}{\Omega}(-\mathrm{i})^2 \int_\Omega \int_\Omega \mathrm{e}^{-\mathrm{i}p\cdot(r-r')} G_{\mathrm{ep}}(rt, rt; r't^+, r't^+)\,\mathrm{d}r\,\mathrm{d}r'$$

$$= \frac{\pi r_0^2 c}{\Omega} \sum_{i_{\mathrm{occ}}} \left| \int_\Omega \mathrm{e}^{-\mathrm{i}p\cdot r} \psi_i^{\mathrm{ep}}(r, r)\,\mathrm{d}r \right|^2 \qquad (1)$$

and

$$\lambda = \int \rho(\boldsymbol{p})\,\mathrm{d}\boldsymbol{p} = \pi r_0^2 c(-\mathrm{i})^2 \int_\Omega G_{\mathrm{ep}}(\boldsymbol{r}t, \boldsymbol{r}t; \boldsymbol{r}t^+, \boldsymbol{r}t^+)\,\mathrm{d}\boldsymbol{r}$$

$$= \pi r_0^2 c \sum_{i_{\mathrm{occ}}} \int_\Omega |\psi_i^{\mathrm{ep}}(\boldsymbol{r}, \boldsymbol{r})|^2\,\mathrm{d}\boldsymbol{r} \tag{2}$$

respectively. Here r_0, c and Ω are the classical electron radius, velocity of light, and volume of the sample, respectively. $\psi_i^{\mathrm{ep}}(\boldsymbol{r}_\mathrm{e}, \boldsymbol{r}_\mathrm{p})$ in equations (1) and (2) are the pair wave functions of the thermalized positron at $\boldsymbol{r}_\mathrm{p}$ and the electron in the *initial* state i at $\boldsymbol{r}_\mathrm{e}$ and G_{ep} is the zero-temperature electron–positron Green's function related to $\psi_i^{\mathrm{ep}}(\boldsymbol{r}_\mathrm{e}, \boldsymbol{r}_\mathrm{p})$ as

$$G_{\mathrm{ep}}(\boldsymbol{r}_\mathrm{e}t, \boldsymbol{r}_\mathrm{p}t; \boldsymbol{r}'_\mathrm{e}t^+, \boldsymbol{r}'_\mathrm{p}t^+) = (-\mathrm{i})^2 \sum_{i_{\mathrm{occ}}} [\psi_i^{\mathrm{ep}}(\boldsymbol{r}_\mathrm{e}, \boldsymbol{r}_\mathrm{p})]^* \psi_i^{\mathrm{ep}}(\boldsymbol{r}'_\mathrm{e}, \boldsymbol{r}'_\mathrm{p}) \tag{3}$$

(for more details see appendix). Summation in (1)–(3) runs over all occupied initial electronic states i.

The slow-positron beam technique enables us to measure the SS positron lifetime $\tau = 1/\lambda$ and 2D or 1D projections of $\rho(\boldsymbol{p})$, i.e.

$$N(p_x, p_z) = \xi \int \rho(\boldsymbol{p})\,\mathrm{d}p_y$$

$$N(p_z) = \int N(p_x, p_z)\,\mathrm{d}p_x \qquad N(p_x) = \int N(p_x, p_z)\,\mathrm{d}p_z$$

where ξ is a normalization constant.

It is apparent that when one determines positron annihilation characteristics $\rho(\boldsymbol{p})$ and λ, the knowledge of $G_{\mathrm{ep}}(\psi_i^{\mathrm{ep}})$ is necessary, at least for $\boldsymbol{r}_\mathrm{e} = \boldsymbol{r}_\mathrm{p}$. This problem, however has not yet been solved for a real metallic system.

In the region of strongly varying density (at the metal surface), the pair wave functions $\psi_i^{\mathrm{ep}}(\boldsymbol{r}_\mathrm{e}, \boldsymbol{r}_\mathrm{p})$ may be approximated in the form (for more details see [17] and [20])

$$\psi_i^{\mathrm{ep}}(\boldsymbol{r}_\mathrm{e}, \boldsymbol{r}_\mathrm{p}) = \psi_+(\boldsymbol{r}_\mathrm{p})\psi_i^0(\boldsymbol{r}_\mathrm{e})[1 + \Delta\rho(\boldsymbol{r}_\mathrm{e}; \boldsymbol{r}_\mathrm{p}, Q = 1)/n_{\mathrm{el}}(\boldsymbol{r}_\mathrm{e})]^{1/2} \tag{4}$$

where $\psi_i^0(\boldsymbol{r}_\mathrm{e})$ are the electron wave functions in the host material (in the absence of a positron), $\psi_+(\boldsymbol{r})$ stands for a positron wave function and

$$n_{\mathrm{el}}(\boldsymbol{r}) = \sum_{i_{\mathrm{occ}}} |\psi_i^0(\boldsymbol{r})|^2 \tag{5}$$

is the electron density in the host material. The electron–positron interaction parameter Q in equation (4) may be understood as the charge of a light particle embedded in the many-electron system and

$$\Delta\rho(\boldsymbol{r}_\mathrm{e}, \boldsymbol{r}_\mathrm{p}, Q = 1) = \sum_{i_{\mathrm{occ}}} |\psi_i^{\mathrm{ep}}(\boldsymbol{r}_\mathrm{e}, \boldsymbol{r}_\mathrm{p})|^2 / |\psi_+(\boldsymbol{r}_\mathrm{p})|^2 - n_{\mathrm{el}}(\boldsymbol{r}_\mathrm{e}) \tag{6}$$

denotes the conditional electronic screening charge density at $\boldsymbol{r}_\mathrm{e}$ assuming that the positron is at $\boldsymbol{r}_\mathrm{p}$. For any positron position $\boldsymbol{r}_\mathrm{p}$ the charge-neutrality condition

$$\int \Delta\rho(\boldsymbol{r}_\mathrm{e}; \boldsymbol{r}_\mathrm{p}, Q)\,\mathrm{d}\boldsymbol{r}_\mathrm{e} = Q. \tag{7}$$

should be satisfied ([17] and references cited therein).

The electron wave functions $\psi_i^0(r)$ are usually determined within the Hohenberg–Kohn–Sham formalism [37, 38] as the solutions of the set of one-particle Schrödinger equations with an effective potential $V_-(r_e) = V_C(r_e) + V_{xc}(r_e)$, which consists of the Coulomb (V_C) and electron–electron correlation–exchange (V_{xc}) parts. The Coulomb potential V_C and electron density n_{el} generate each other, according to equation (5) and the Poisson equation.

The positron wave function is an eigenfunction of the Schrödinger equation with the potential $V_+(r) = -V_C(r) + V_{corr}(r)$ being the sum of the electron Coulomb (with opposite sign) and electron–positron correlation potentials, $-V_C$ and V_{corr}, respectively (cf, e.g. [18 19, 22, 23, 26–29, 39–41]). Potential energy seen by electrons and positrons at a surface is schematically shown in figure 1.

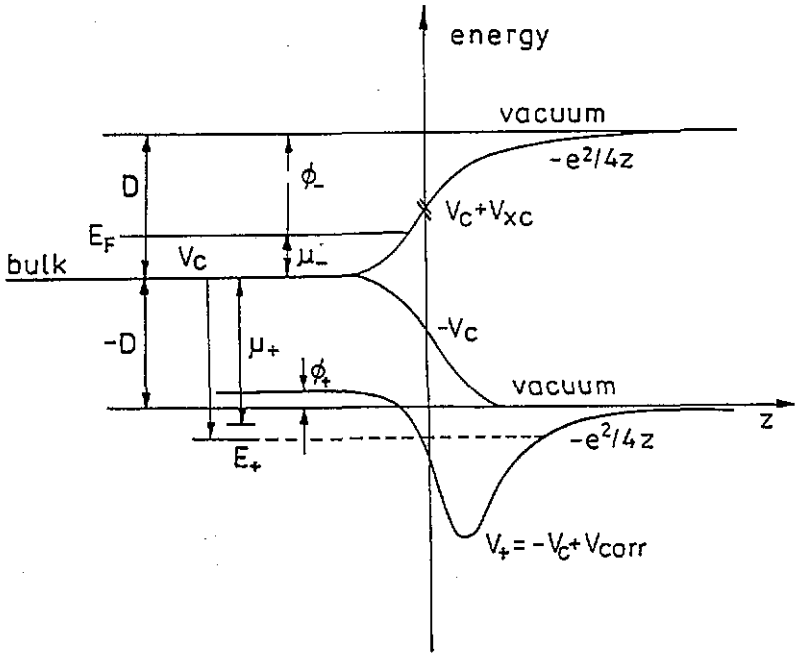

Figure 1. Potential energy as seen by electrons and positrons at a surface.

The correlation potential $V_{corr}(r_p)$ should be thought of as the work done to bring the positron to r_p against the Coulomb forces between the positron and electronic polarization cloud and is determined by the form of screening charge distribution $\Delta\rho(r_e; r_p, Q)$. In the calculations of the present work the approach based on the Feynman theorem is used (for more details see [17]). The correlation potential acting on the positron located at r_p can be expressed as

$$V_{corr}(r_p) = -\int_0^1 dQ \int \Delta\rho(r_e; r_p, Q)/|r_e - r_p|\, dr_e. \tag{8}$$

Within the approximation (4) partial and total annihilation rates for a positron trapped at the surface read as

$$\rho(p) = \frac{\pi r_0^2 c}{\Omega} \sum_{i_{occ}} \left| \int_\Omega e^{-ip\cdot r} \psi_+(r) \psi_i^0(r) [1 + \Delta\rho(r; r, Q = 1)/n_{el}(r)]^{1/2}\, dr \right|^2 \tag{9}$$

$$\lambda = \pi r_0^2 c \int |\psi_+(r)|^2 n_{el}(r)[1 + \Delta\rho(r; r, Q = 1)/n_{el}(r)]\,dr. \tag{10}$$

If the quasi-IPM is applied [18 19, 21–23], $\Delta\rho(r; r, Q)$ in equations (9) and (10) is set equal to zero (while V_{corr} in the positron Schrödinger equation is not constant, in disagreement with equation (8); internal consistency of this model is discussed in [17] and [20]).

When the present approximations (4), (9) and (10) are used, the problem of determining positron annihilation characteristics at the surface reduces to the knowledge of electron wave functions in the host material, $\psi_i^0(r_e)$ (which determine $n_{el}(r_e)$ according to equation (5)), the positron wave function $\psi_+(r_p)$ and the screening charge distribution $\Delta\rho(r_e; r_p, Q)$, at least for $r_e = r_p$.

2.1. Unperturbed electron wave functions at the surface

As shown on mathematical grounds [30], from the point of view of annihilation characteristics $\rho(p)$ inside the central Fermi sphere and λ, valence electrons in the bulk simple metals are described within the jellium model reasonably well, except the momenta close to the Brillouin zone boundary. This property should be conserved parallel to the surface plane. Within this model the ions are thought of as forming the positive background charge within the metal, $n_{ion}(z) = n_0\theta(-z)$, where θ is the unit-step function and $n_0 = 3/(4\pi r_s^3)$ is the average electron density in the bulk material. The resulting electron and positron potentials, $V_-(r_e)$ and $V_+(r_p)$, vary only in the direction normal to the surface and the electron and positron wave functions, labelled by the wavevector k are considered to be of the form

$$\psi_k^0(r) = S^{-1/2}\exp[i(k_x x + k_y y)]\psi_{k_z}(z) \tag{11}$$

$$\psi_+(r) = S^{-1/2}\psi_+(z) \tag{12}$$

where $r = (x, y, z)$, the z axis is normal to the surface and S is the area of the surface plane. The boundary conditions for $\psi_{k_z}(z)$ are $\psi_{k_z}(z) = \sin[k_z z - \delta(k_z)]$ for $z \to -\infty$, where $\delta(k_z)$ is the phase shift, and $\psi_{k_z}(\infty) = 0$. In this way the self-consistent solution of the 3D Hohenberg–Kohn–Sham equations can be reduced to the solution of a 1D problem.

The calculations of the electron wave functions $\psi_{k_z}(z)$ and Coulomb potentials $V_C(z)$ were performed for surfaces of Al($r_s = 2.07$), Cd($r_s = 2.571$), Mg($r_s = 2.638$), Li($r_s = 3.241$), Na($r_s = 3.931$) and K($r_s = 4.862$) using the modified Monnier–Perdew computer codes [33,42]. The electron–electron exchange–correlation potential V_{xc}, following from the self-consistent matching procedure of Serena *et al* [43] (see also [33]) is applied. In this method the LDA exchange–correlation potential in the metal is matched at the image plane z_I, to the non-local potential of the form:

$$V_{xc}^{NL}(z) = -\{1 - [1 + b(z - z_I)/4]e^{-b(z-z_I)}\}/4(z - z_I) \tag{13}$$

where $b = -(16/3)V_{xc}(z_I)$ is determined self-consistently from the condition of continuity of V_{xc} at z_I. For the electron–electron correlation energy inside the metal we employ the parametrized Ceperley–Alder values [44, 45].

2.2. Electron–positron correlation effects and the positron wave function

The screening charge distribution $\Delta\rho(r_e; r_p, Q)$ and, following from it, the electron–positron correlation potential V_{corr} (equation (8)) were modelled within the WDA [17, 25, 26]. The WDA is in principle an adaption of the LDA to strongly inhomogeneous systems.

The difference between the WDA and the LDA consists in replacing the displaced-charge correlation function, $1 + \Delta\rho(r_e; r_p, Q)/n_{el}(r_e)$, by its analog in an electron gas of some effective electron density $n^*(r_p)$, instead of $n_{el}(r_p)$ as employed within the LDA. The values of the density $n^*(r_p)$ are determined for any positron position r_p from the charge-neutrality condition (7), which is treated as an equation for $n^*(r_p)$. The switch from n_{el} to n^* may be understood as inclusion of non-local correlation effects.

In the present work $\Delta\rho(r_e; r_p, Q)$ is assumed to be of the form

$$\Delta\rho(r_e, r_p, Q) = Qn_{el}(r_e)\{a^3[n^*(r_p)]/8\pi n^*(r_p)\}\exp\{-a[n^*(r_p)]|r_e - r_p|\} \tag{14}$$

where the Brandt–Reinheimer [46] parametrization of $a(n^*)$ is used.

When one considers the real metal surface, the difference potential $\delta v_+(r)$ should be added to $V_+(z)$ in order to reproduce correctly energy levels in the bulk, which is, otherwise poorly represented by the potential of the uniform positive background of ions. In this work $\delta v_+(r)$ is replaced by a constant value $\langle\delta v_+\rangle$ for $z \leqslant -d/2$ by the linear function $-2z\langle\delta v_+\rangle/d$ for $-d/2 \leqslant z \leqslant 0$ and by zero for $z \geqslant 0$, where d is the interplanar distance averaged over the main crystallographic directions. The value of $\langle\delta v_+\rangle$ is chosen in such a way that inside the metal

$$-V_C(-\infty) + V_{corr}(-\infty) + \langle\delta v_+\rangle = -\phi_+$$

where ϕ_+ is the positron work function.

The electron (positron) work function for a solid is defined as the minimum energy required to remove an electron (positron) from the point inside the bulk to one in the vacuum. This includes a bulk contribution, which is the electron (positron) chemical potential μ_- (μ_+), and a surface contribution D, which is called the surface dipole barrier, (cf e.g. [1, 4]),

$$\phi_- = D - \mu_- \tag{15a}$$

$$\phi_+ = -D - \mu_+ = -(\mu_+ + \mu_-) - \phi_- = -\Sigma - \phi_- \tag{15b}$$

respectively, where $\Sigma = \mu_+ + \mu_-$. For metals μ_- is equal to the absolute value of the Fermi energy and μ_+ is the lowest energy of the positron energy band (see figure 1).

The reference level for the potential μ_+ must be *the same* as that used in calculating μ_- (cf. e.g. [4, 39–41]). In the present work the electron and positron chemical potentials were obtained within LMTO ASA, following the formalism of [29]. The electron atomic potentials were determined relativistically using the code of Liberman *et al* [47] with the local exchange–correlation potential in the Hedin–Lundqvist form. The solid-state electron configurations of [49] and [50] (cf columns 3 and 4 of table 1) were applied. The Coulomb potential in the lattice was generated by superposition of atomic electron densities within the Mattheiss [51] construction scheme. In the calculations of μ_+, the local electron–positron correlation potential in the form parametrized in [52] was taken into account. The zero of the electron Coulomb potential at the Wigner–Seitz sphere was set as the zero energy level in both positron and electron models.

3. Results and discussion

The electron work functions ϕ_-^{th} in Al, Mg, Cd, Na and K, obtained in the present work are compared with experimental data [53] in table 1 (columns 9 and 10, respectively). It should be noted here that all our calculations of annihilation parameters at the surface are performed twice: on the basis of the values of ϕ_-^{th} and ϕ_-^{exp} separately, and two sets of results are presented.

Table 1. Energy components of the positron work function ϕ_+. The electron work functions ϕ_- calculated in this work (column 9) are compared with experimental data [53] (column 10). In columns (5)–(8) the values of energy $\Sigma = (\mu_+ + \mu_-)$ obtained (a) in the present work, (b) by Fletcher *et al* [41], (c) by Farjam and Schroe [40] and (d) by Boev *et al* [39] are presented.

		Configuration		$-\Sigma$ (eV)				ϕ_- (eV)	
Metal	r_s	s	p	(a)	(b)	(c)	(d)	This work	Exp.
Al	2.07	1.59	1.41	3.82	5.25	4.43	4.09	3.89	4.28
Cd	2.57	1.18	0.82	4.27	6.40	—	—	3.61	4.10
Mg	2.64	0.81	1.19	6.23	7.04	6.63	—	3.58	3.66
Li	3.24	0.53	0.47	7.53	8.48	7.80	—	3.30	2.90
Na	3.93	0.75	0.25	7.60	8.45	7.69	7.12	2.99	2.75
K	4.86	0.67	0.33	7.53	2.82	7.63	7.05	2.70	2.30

The values of energy Σ, necessary in studies of the positron work function ϕ_+, resulting from various approaches are listed in columns 5–8 of table 1. It should be remembered that the present calculations and the ones of Boev *et al* [39] are based on the LMTO ASA [50, 54], while Fletcher *et al* [41] and Farjam and Schroe [40] take advantage of the work of Moruzzi *et al* [55]. The discrepancies between theoretical results for Σ, observed in table 1, can also be attributed to the differences in the lattice constants a used in the band-structure calculations (our values of a, which determine the electron density parameter r_s, are taken from [49, 50]).

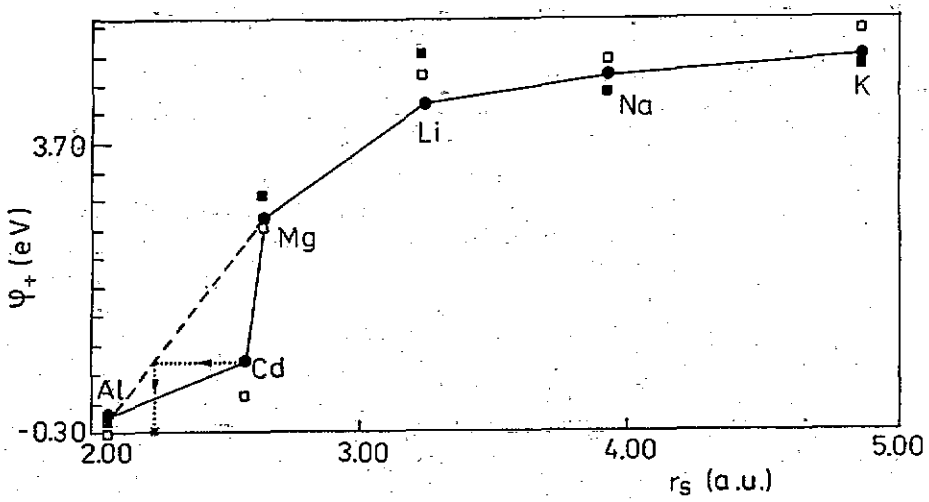

Figure 2. Positron work function as a function of r_s obtained according to equation (15*b*), with ϕ_-^{th} as obtained in this work (full circles connected by a solid line) and ϕ_-^{exp} (empty squares) compared with the theoretical results of Boev *et al* [39] for Al, Na and K of Farjam and Schroe [40] for Mg and Li (black squares). The broken line connects jellium-like metals and the dotted lines show how the 'effective' electron density parameter in cadmium (asterisk) is determined, as described in the text.

The positron work functions, calculated according to equation (15*b*), are presented in figure 2 as a function of the electron density parameter r_s. The results of [39] and [40] are quoted in figure 2 for comparison. According to our best knowledge, the experimental values of ϕ_+ are available for Al low-index faces only ($\phi_+^{exp} = -0.19$ eV at the (100);

−0.05 eV at (110); and −0.04 eV at (111) surface), while for Cd ϕ_+^{exp} is known to be positive (cf [1, 2]).

The distribution of electronic charge screening a positron located at r_p and the electron–positron correlation potential were modelled within the WDA, according to equations (7), (8) and (14). For positron positions z_p well inside the metal, the values of the effective WDA electron density $n^*(z_p)$ coincide with $n_{el}(z_p)$. When the positron is in the vacuum ($z_p \to \infty$), $n_{el}(z_p)/n^*(z_p) \to 0$. The screening cloud, which is spherically symmetric in the bulk, deforms as the positron approaches the surface and is left behind at the image plane located at z_I for positron positions far in the vacuum. Asymptotic behaviour of $V_{corr}(z_p) \to -1/[2(z_p - z_I)]$ is observed and the potential well is formed in the near-surface region. These results are difficult to obtain within the LDA.

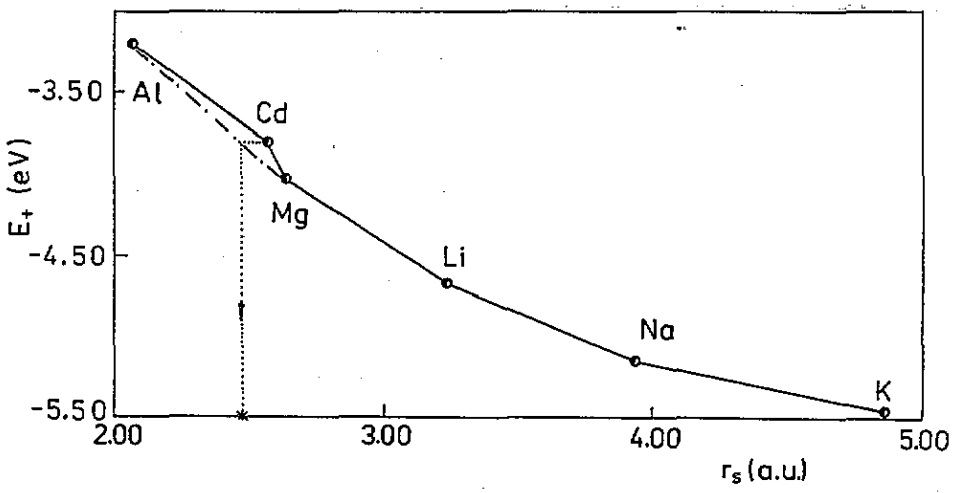

Figure 3. Ground-state energy eigenvalues of the positron Schrödinger equation as a function of r_s. The chain line connects jellium-like metals, while the dotted lines and the asterisk have the same meaning as in figure 2.

The positron ground-state energies E_+ (referenced to the vacuum level) are shown in figure 3 as a function of the bulk electron density parameter r_s. In contrast to the positron work function, E_+ appears not to be sensitive to the switch from ϕ_-^{exp} to ϕ_-^{th} in the model. The resulting value of binding energy (relative to the bulk) for a positron trapped at the Al surface is in good agreement with experimental data for the Al(100) face, $E_B = -3.05$ eV [1] or −2.8 eV [2].

Except for Al, the positron work functions take positive values in the metals under study (cf figure 2 and table 1). This result could suggest positron trapping inside the metal. This is not the case, however, because the positron energies E_+ are lower than $-\phi_+$ (compare figures 2 and 3), and the positron is localized inside the potential well at the surface. The positron distributions at the surfaces under study are presented in figure 4.

In Al and Cd the major part of the positron distribution is found on the vacuum side. With increasing values of r_s, the peak of $\psi_+(z)$ moves to the metal and portion of the positron wave function found in the metal side of the surface plane becomes non-negligible. This fact is reflected in the positron lifetime at the surface, calculated according to equation (10). In figure 5 the values of τ obtained within the present formalism are compared with experimental lifetime data in the bulk. It is apparent that with decreasing

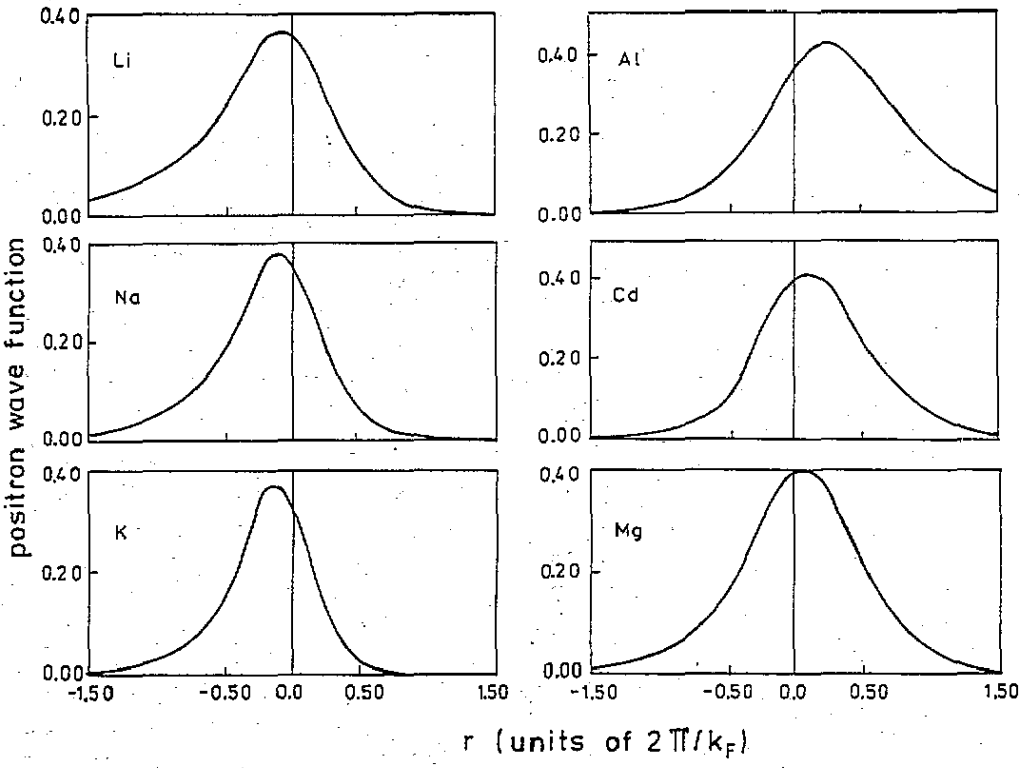

Figure 4. Positron distributions at a surface.

electron density in bulk, the SS positron lifetime becomes more and more bulk-like. In our opinion, this result is mainly due to the shape of the positron wave function at the surface.

In Al and Cd the values of τ exceed the spin-averaged free positronium value of 500 ps. Theoretical results for Al (580 and 590 ps for models based on ϕ_-^{th} and ϕ_-^{exp}, respectively) are in excellent agreement with experimental data of Lynn *et al* [15], $\tau^{\text{exp}} = 580$ ps at the Al(110) surface. In Cd the lifetimes obtained within the two models amount to 538 and 555 ps, respectively.

The 'regular' shape of $\phi_+(r_s)$, $E_+(r_s)$ and $\tau(r_s)$ is broken at Cd (compare solid and broken lines in figures 2, 3 and 5). This behaviour of SS positron annihilation parameters in cadmium is not quite unexpected. The band structure calculation results show (see, e.g. [49,55]) that Cd is difficult to treat as a free-electron metal since the core d band in cadmium lies close to the bottom of the conduction band. This feature is reflected in the energy parameter Σ and, through the positron work function ϕ_+, in E_+ and τ.

On might suggest that, from the point of view of the annihilation characteristics, cadmium could be considered as a free-electron metal if the electron density parameter r_s were replaced by some 'effective' value r_s^{eff}. Recently Kontrym–Sznajd and Daniuk [56] have made an attempt to determine r_s^{eff} in a series of bulk metals. The value of r_s^{eff} in a real metal was extracted from comparison of the bulk lifetime obtained within the LDA [29] with the one following from electron gas theory, in the way schematically shown in the lower part of figure 5 by the dotted lines and by the asterisks on the r_s axis. It should be noted here that this procedure is highly risky, ambiguous and difficult to substantiate at the surface of a real metal, as shown on the example of cadmium. As seen in figures 2, 3

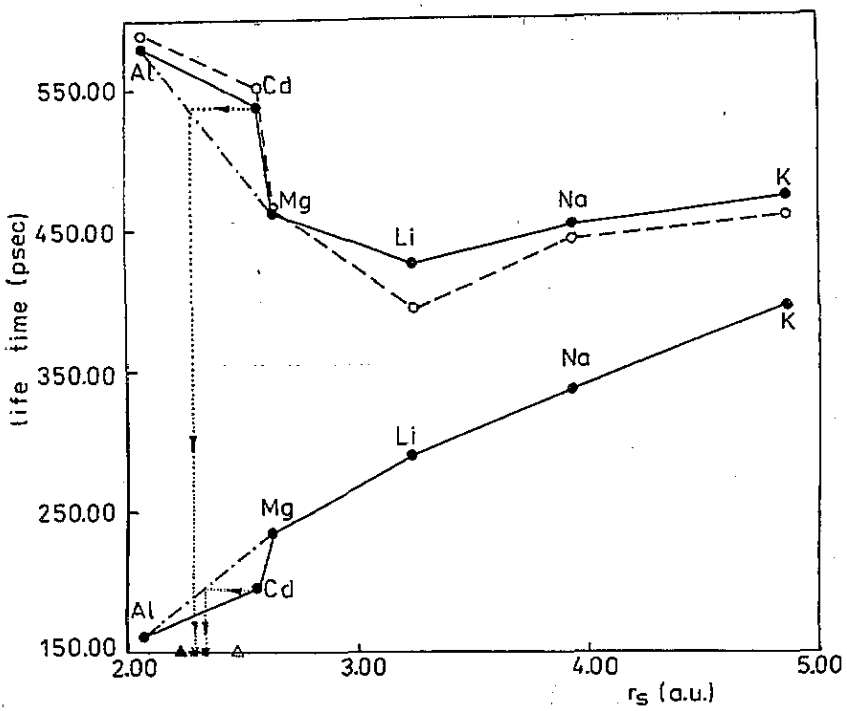

Figure 5. Positron ss lifetime as a function of r_s obtained within the present model using the theoretical electron work function ϕ_-^{th} (upper black circles connected by a solid line) and ϕ_-^{exp} (empty circles connected by a broken line) compared with experimental values of positron lifetime in the bulk (lower black circles connected by a solid line). Chain and dotted lines and asterisks have the same meanings as in figure 2. The black and empty triangles are the 'effective' density parameters based on $\phi_+(r_s)$ (asterisk in figure 2) and $E_+(r_s)$ (asterisk in figure 3), respectively.

and 5 (dotted lines and asterisks as well as the triangles in figure 5), the choice of r_s^{eff} is strongly dependent on the annihilation parameter under study (ϕ_+, E_+ and τ, respectively). Moreover, even in the case when only the positron lifetime is considered, the values of the 'effective' electron density also differ for the bulk and surface characteristics. When one determines annihilation parameters at the surfaces of d-electron metals, no electron density parameter r_s^{eff} applied to the jellium model can describe properly ϕ_+, E_+ and τ simultaneously.

Partial annihilation rates $\rho(p)$ were calculated according to equation (9) with the WDA screening charge given by equation (14). For electron and positron wave functions in the form (11) and (12), the 1D projections of $\rho(p)$, $N(p_x)$ and $N(p_z)$, read as [17]

$$N(p_x) = \alpha_x \int_0^{\kappa} (\kappa^2 - k_z^2)^{1/2}\,dk_z \int_{-\infty}^{\infty} |\psi_{k_z}(z)|^2 |\psi_+(z)|^2 \{1 + a^3[n^*(z)]/[8\pi n^*(z)]\}\,dz \quad (16a)$$

$$N(p_z) = \alpha_z \int_0^{k_F} (k_F^2 - k_z^2)\,dk_z \left| \int_{-\infty}^{\infty} e^{ip_z z} \psi_{k_z}(z)\psi_+(z)\{1 + a^3[n^*(z)]/[8\pi n^*(z)]\}^{1/2}\,dz \right|^2 \quad (16b)$$

where α_x and α_z are the normalization constants, k_F denotes the Fermi momentum in the bulk and $\kappa = (k_F^2 - p_x^2)^{1/2}$.

The 1D momentum distributions $N(p_z)/N(p_z = 0)$ and $N(p_x)/N(p_x = 0)$ in Al, Cd, Mg, Li, Na and K are represented in figure 6 by broken and solid lines, respectively.

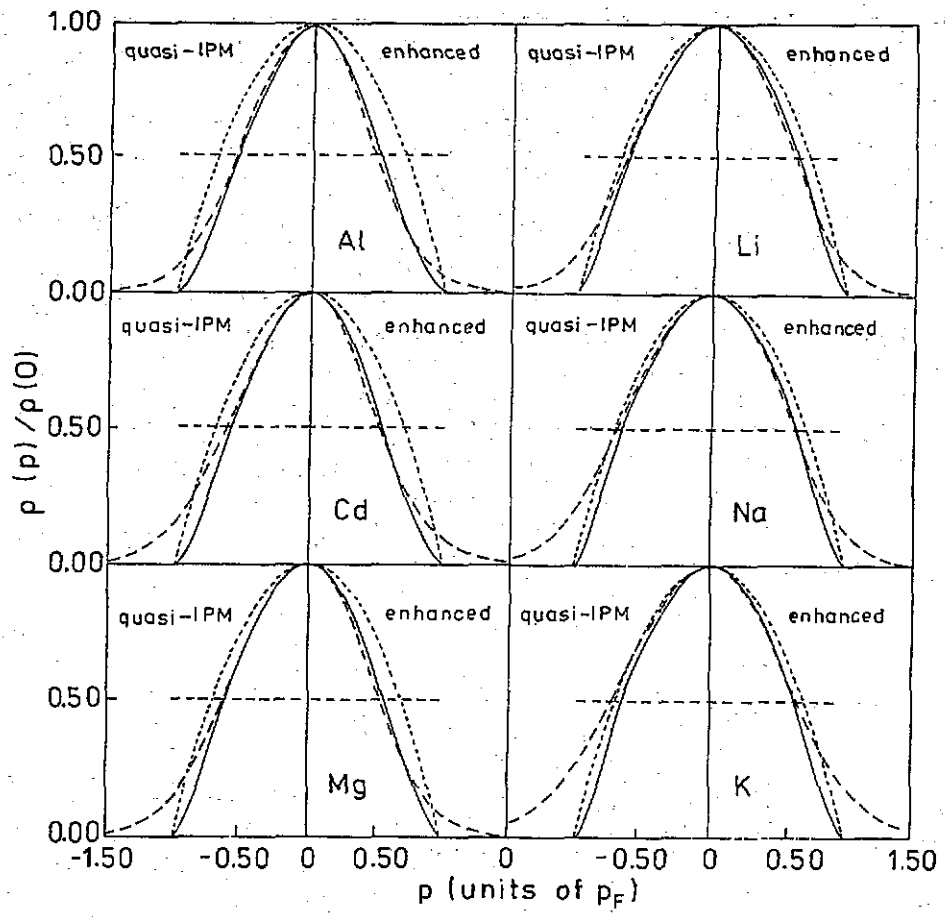

Figure 6. 1D momentum distributions $N(p_z)$ (long-dashed curves) and $N(p_x)$ (solid curves) obtained within quasi-IPM (left portions of graphs) and enhanced models (right portions of graphs). The inverted parabola, corresponding to bulk material, is denoted by the short-dashed curves. The full widths at half maximum are marked by the horizontal lines.

Their quasi-IPM analogs, obtained according to formulae (16) with $a^3[n^*(z)] \equiv 0$ (i.e. for $\Delta\rho(\boldsymbol{r}_e; \boldsymbol{r}_p, Q) \equiv 0$ but with $V_{corr}(\boldsymbol{r}_p) \neq$ const) are given in figure 6 for comparison. The inverted parabola $1-p^2$ (which corresponds to the momentum distribution of the nearly-free electrons in the bulk) is given as a dotted line. Momenta are expressed in units of the Fermi momentum k_F.

It is apparent that including electron–positron correlations causes narrowing of theoretical ACAR spectra and decreases anisotropy with respect to quasi-independent particles model (IPM). For Al the agreement between theory and experiment ([9, 10]) is appreciably improved when the electron–positron correlations are taken into account in the ACAR formulae (16) (see also [17]). The discrepancies between theory and experiment are pronounced for momenta close to the Fermi momentum and higher. This is obviously the result of neglect of lattice effects when the form (11) of the electron wave functions at the real metal surface is considered.

Except for K, all the spectra obtained within the enhanced model are almost isotropic, with the normal component slightly narrower than the parallel one. As the density parameter

r_s increases, the ACAR spectra become more and more bulk-like (compare differences between the solid and dashed lines in Al and K). This feature, which is common for the SS momentum distributions and lifetimes (see relation between $\rho(p)$ and λ), should be attributed to the fact that the probability of finding the surface positron inside the metal increases when the positron work function becomes more and more positive.

Since quasi-IPM ACAR spectra must not be related directly to experimental ones, in the interpretation of slow-positron annihilation data the knowledge of momentum-dependent enhancement factors $\epsilon(p) = \rho(p)/\rho^{\mathrm{IPM}}(p)$ is needed. The resulting quasi-IPM ACAR spectra are anisotropic, and therefore it seems to be more reasonable to consider two separate parameters $\epsilon(p_z) = N(p_z)/N^{\mathrm{IPM}}(p_z)$ and $\epsilon(p_x) = N(p_x)/N^{\mathrm{IPM}}(p_x)$, instead of the isotropic one, $\epsilon(|p|)$, often used on the case of bulk metal (for reviews see, e.g. [30,36]). In figure 7 the parameters $\epsilon(p_x)/\epsilon(p_x = 0)$ and $\epsilon(p_z)/\epsilon(p_z = 0)$ are shown by solid and broken lines, respectively. In Al the reasonable agreement between $\epsilon(p_z)$ and the 'experimental' enhancement factor, extracted from [10] is found. Since for momenta $p_x \geqslant k_F$ both $N(p_x)$ and $N^{\mathrm{IPM}}(p_x)$, obtained according to equation (16*a*) are equal to zero, enhancement factors $\epsilon(p_x)$ are well-defined only for $p_x < k_F$.

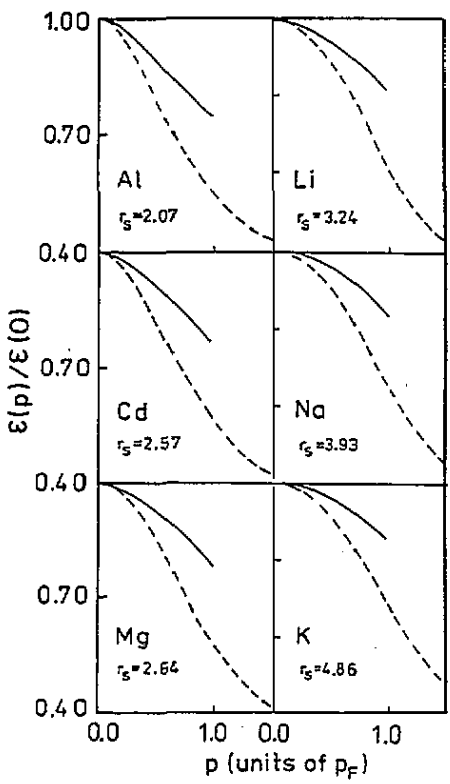

Figure 7. Momentum-dependent enhancement factors at a surface, $\epsilon(p_z)/\epsilon(p_z = 0)$ (broken curves) and $\epsilon(p_x)/\epsilon(p_x = 0)$ (solid curves).

In all the metals under study, both $\epsilon(p_x)$ and $\epsilon(p_z)$ are decreasing functions of momentum, as the enhanced ACAR spectra are narrower than the quasi-IPM ones (in the bulk metal the enhancement factors for nearly parabolic valence bands are always increasing functions of momentum, see e.g. [30,36]). On the other hand, the decrease of $\epsilon(p)$ for strongly varying electron densities (e.g. the metal surface) is in agreement with theoretical

predictions of $\epsilon(p)$ for localized electrons in the bulk, where the negative slope of $\epsilon(p)$ was found for core [29,57] and d [32] electrons.

For all the metals presented in figure 7, enhancement factors $\epsilon(p_z)$ exhibit a stronger tendency to decrease than $\epsilon(p_x)$. This feature may be attributed to the following factors.

(i) The enhanced spectra are almost isotropic with the parallel component slightly broader than the normal one, while for any of quasi-IPM densities the parallel component is narrower than the perpendicular one.

(ii) As shown on mathematical grounds, based on the electronic band-structure calculations in the bulk [30,31], the higher the degree of localization of electronic population in a real metal, the stronger the tendency $\epsilon(p)$ shows to decrease. Comparison of $\epsilon(p_x)$ and $\epsilon(p_z)$ clearly indicates that the electron wave functions in the host material are more strongly localized normal to the surface plane than parallel to it. This conclusion is well justified by the form (11) of $\psi_k^0(r)$.

4. Conclusions

Annihilation characteristics for positrons trapped at the surfaces of simple metals and Cd are studied. Theoretical results for the positron lifetime and ACAR spectrum from the Al surface, obtained within the proposed approach, are found to be in fairly good agreement with experimental data [9, 10] and [15] in spite of the fact that the calculations are performed within a crude approximation to the electron wave functions and to the pseudopotential of ions inside the metal. Inclusion of electron–positron enhancement effects appreciably improves the agreement between theory and experiment in Al, in comparison with quasi-IPM. Unfortunately, the slow-positron experiment has not been performed on the surfaces of other simple metals, due to technical problems [16], and practical verification of the present theory is still required.

Positron energy and lifetime at the surface are found to be decreasing functions of the bulk density parameter r_s, while the positron work function increases with r_s. This behaviour of $\phi_+(r_s)$ is well justified by the fact that in nearly free electron metals, the electron chemical potential in the bulk (equal to the Fermi energy E_F) is approximately proportional to r_s^{-2}.

As the average electron density in the bulk metal decreases, the lifetime and ACAR spectra for a positron in the SS become more and more bulk-like. This feature may be attributed to the localization of the positron potential well, determining the positron annihilation characteristics through the positron distribution at the surface.

Electron–positron enhancement factors at the surfaces of simple metals and cadmium appear to be decreasing functions of momentum. The normal components $\epsilon(p_z)$ show a stronger tendency to decrease than $\epsilon(p_x)$. This result indicates that the electrons are more strongly localized normal to the surface than parallel to it, in agreement with expectations. It should be stressed here that the degree of localization of electrons, clearly observed in the enhancement factors (for more detailed discussion see [30] and [31]), is difficult to deduce from the shape of the surface ACAR spectra. This fact might have been the reason for the controversial conclusions drawn by other authors (cf e.g. [18, 19, 23]) that the isotropic shape of ACAR spectra from the Al surfaces [9, 10] is in disagreement with delocalization of valence electrons parallel to the surface plane.

The surface positron parameters are found to be sensitive to the electron band structure in the bulk. The difference between the electronic properties in bulk cadmium and free-electron metals is reflected in the positron work function, binding energy and lifetime. This

result leads to the conclusion, that in d-electron metals the exact electron band-structure calculations are necessary in the interpretation of positron annihilation characteristics at the surface. Without doubt any 'universal' effective electron density parameter r_s^{eff}, reproducing properly at the same time the positron work function, surface energy and lifetime as $\phi_+(r_s^{\text{eff}})$, $E_+(r_s^{\text{eff}})$ and $\tau(r_s^{\text{eff}})$ in the free-electron metals, cannot be found in the d-electron metals, as clearly follows from fitting data for Cd to broken lines in figures 2, 3 and 5. It should be added here that seeking the effective electron density parameters on the basis of the total annihilation rates in real bulk metals [56] is also controversial, even for the valence electrons in simple metals. The values of the 'effective' electron density parameters based on various annihilation characteristics (e.g. λ, λ^{IPM}, $\epsilon(p)$) are usually different or impossible to determine.

Acknowledgments

AR is grateful to Professor W Triftshauser for helpful remarks concerning difficulties with the slow-positron experiment on the surfaces of simple metals. AR and AK would like to thank Renè Monnier for helpful discussions on the properties of the host metal surface.

Appendix

Let us consider the one-positron N-electron system in the ground state $|0\rangle$ described by the wave function

$$|0\rangle = \Phi_{\text{ep}}(r_{\text{p}}, r_1, \ldots, r_N). \tag{A1}$$

The Green's function of the system reads as

$$\begin{aligned} G_{\text{ep}}(r_{\text{e}}t, r_{\text{p}}t; r'_{\text{e}}t^+, r'_{\text{p}}t^+) &= (-\text{i})^2\langle 0|T[\psi_{\text{e}}(r_{\text{e}}t)\psi_{\text{p}}(r_{\text{p}}t)\psi^\dagger_{\text{e}}(r'_{\text{e}}t^+)\psi^\dagger_{\text{p}}(r'_{\text{p}}t^+)]|0\rangle \\ &= (-\text{i})^2\langle 0|\psi^\dagger_{\text{e}}(r'_{\text{e}})\psi^\dagger_{\text{p}}(r'_{\text{p}})\psi_{\text{e}}(r_{\text{e}})\psi_{\text{p}}(r_{\text{p}})|0\rangle \\ &= \frac{(-\text{i})^2}{N}\int \text{d}r_2 \ldots \text{d}r_N\, \Phi_{\text{ep}}(r_{\text{p}}, r_{\text{e}}, r_2, \ldots, r_N)]^* \Phi_{\text{ep}}(r'_{\text{p}}, r'_{\text{e}}, r_2, \ldots, r_N) \end{aligned} \tag{A2}$$

where T is the Wick's operator and ψ ($\psi^\dagger$) are the annihilation (creation) operators.

Within the independent particles model (IPM) formula (3) follows directly from the fact that Φ_{ep} is the product of the positron wave function and the Slater determinant of unperturbed electron wave functions $\psi_i^0(r_j)$, where i are the lowest energy (occupied) states, i.e.

$$\Phi^{\text{IPM}}_{\text{ep}}(r_{\text{p}}, r_1, \ldots, r_N) = \psi_+(r_{\text{p}})(N!)^{-1/2}\det[\psi_i^0(r_j)]. \tag{A3}$$

This determinant may be expanded with respect to the first column as

$$\det[\psi_i^0(r_j)] = \sum_{m=1}^{N}(-1)^{m+1}\psi^0_{i_m}(r_1)\det[\psi_i^0(r_j)]_{\substack{j=2\ldots N \\ i\neq i_m}} = \sum_{i_{\text{occ}}}\psi_i^0(r_1)f_i(r_2 \ldots r_N). \tag{A4}$$

Since ψ_i^0 are orthogonal, i.e.

$$\langle \psi_i^0|\psi_j^0|\rangle = \delta_{ij} \tag{A5}$$

$$\langle f_i|f_j\rangle = \int \text{d}r_2 \ldots \text{d}r_N[f_i(r_2 \ldots r_N)]^* f_j(r_2 \ldots r_N) = (N-1)!\delta_{ij}. \tag{A6}$$

As a result of (A3)–(A6), integration in (A2) simplifies to

$$G_{ep}^{IPM}(r_e t, r_p t : r'_e t^+, r'_p t^+) = (-i)^2 \sum_{i_{occ}} [\psi_+(r_p)\psi_i^0(r_p)]^* \psi_+(r'_p)\psi_i^0(r'_e)$$

which provides equation (3) with $\psi_i^{ep}(r_e, r_p) = \psi_+(r_p)\psi_i^0(r_e)$.

In the interacting system the wave function Φ_{ep} may be written in the form

$$\Phi_{ep}(r_p, r_1, \ldots, r_N) = \psi_+(r_p)\Phi_e(r_1, \ldots, r_N; r_p) \tag{A7}$$

where

$$|\psi_+(r_p)|^2 = \int dr_1 \ldots dr_N |\Phi_{ep}(r_p, r_1, \ldots, r_N)|^2$$

and $\Phi_e(r_1, \ldots, r_N; r_p)$ is the conditional N-electron wave function for a positron at r_p. Similarly as in the case of IPM, we have the N-fermion function which may be written as a Slater determinant of the conditional quasi-particle wave functions $\phi_i(r_j; r_p)$. Here

$$\begin{aligned} \phi_i(r_e; r_p) &= \psi_i^{ep}(r_e, r_p)/\psi_+(r_p) \\ \phi_i(r_e; r_p) &= \psi_i^0(r_e) + \delta\psi_i(r_e; r_p). \end{aligned} \tag{A8}$$

The perturbative terms $\delta\psi_i$ are orthogonal to ψ_j^0 and therefore

$$\langle\phi_i|\phi_j\rangle = \int dr[\phi_i(r; r_p)]^* \phi_j(r; r'_p) = \delta_{ij} + \int dr[\delta\psi_i(r; r_p)]^* \delta\psi_j(r; r'_p). \tag{A9}$$

Since perturbation $\delta\psi_i$ is of local character, the non-orthogonal term $\langle\delta\psi_i|\delta\psi_j\rangle$ in (A9) is of the second order of smallness (cf e.g. [36]). If one neglects this term, one gets (cf (A2)–(A6))

$$G_{ep}(r_e t, r_p t; r'_e t^+, r'_p t^+) = (-i)^2 \sum_{i_{occ}} [\psi_+(r_p)\phi_i(r_e; r_p)]^* \psi_+(r'_p)\phi_i(r'_e; r'_p). \tag{A10}$$

Expressions (A8) and (A10) lead to formula (3).

References

[1] Mills A P Jr 1983 *Positron Solid State Physics* ed W Brandt and A Dupasquier (Amsterdam: North-Holland) p 432

[2] Lynn K G 1983 *Positron Solid State Physics* ed W Brandt and A Dupasquier (Amsterdam: North-Holland) p 609

[3] Dupasquier A and Zecca A 1985 *Riv. Nuovo Cimento (Ser. 3)* **8** 1

[4] Schultz A P and Lynn K G 1988 *Rev. Mod. Phys.* **60** 701

[5] West R N 1974 *Positron Studies in Condensed Matter* (London: Taylor and Francis)

[6] Berko S 1989 *Momentum Densities* ed R N Silver and P E Sokol (New York: Plenum)

[7] Lynn K G, Mills A P Jr, West R N, Berko S, Canter K F and Roelling L O 1985 *Phys. Rev. Lett.* **54** 1702

[8] Lynn K G, Mills A P Jr, Roelling L O and Weber M 1986 *Electronic and Atomic Collisions* ed D C Lorenz, W E Meyerhof and J R Peterson (New York: North-Holland) p 227

[9] Chen D M, Berko S, Canter K F, Lynn K G, Mills A P Jr, Roelling L O, Sferlazzo P, Weinert M and West R N 1987 *Phys. Rev. Lett.* **58** 921

[10] Chen D M, Berko S, Canter K F, Lynn K G, Mills A P Jr, Roelling L O, Sferlazzo P, Weinert M and West R N 1989 *Phys. Rev.* B **39** 3966

[11] Howell R H, Meyer P, Rosenberg I J and Fluss M J 1985 *Phys. Rev. Lett.* **54** 1698

[12] Sferlazzo P, Berko S, Canter K F, Chen D M, Lynn K G, Mills A P Jr, Roelling L O, Viescas A and West R N 1987 *Bull. Am. Phys. Soc.* **32** 899

[13] Howell R H, Rosenberg I J, Meyer P and Fluss M J 1987 *Phys. Rev.* B **35** 4555

[14] Sferlazzo P, Berko S, Canter K F, Lynn K G, Mills A P Jr, Roelling L O, Viescas A and West R N 1988 *Phys. Rev. Lett.* **60** 538
[15] Lynn K G, Frieze W E and Schultz P J 1984 *Phys. Rev. Lett.* **52** 1137
[16] Triftshatiser W 1992 Private communication
[17] Rubaszek A 1991 *Phys. Rev.* B **44** 10 857
[18] Brown A P, Walker A B and West R N 1987 *J. Phys. F: Met. Phys.* **17** 2497
[19] Brown A P, Jensen K O and Walker A B 1988 *J. Phys. F: Met. Phys.* **18** L141
[20] Rubaszek A 1989 *J. Phys.: Condens. Matter* **1** 2141
[21] Rozenfeld B, Świątkowski W and Jerie K 1983 *Acta Phys. Pol.* A **64** 93
[22] Lou Yongming 1988 *Phys. Rev.* B **38** 9490
[23] Lou Yongming, Binglin Gu, Jialin Zhu, Hang Lee and Jiajiong Xiong 1989 *J. Phys.: Condens. Matter* **1** 2977
[24] Rubaszek A and Lach J 1989 *J. Phys.: Condens. Matter* **1** 9243; 1989 *Surf. Sci.* **211/212** 227
[25] Gunnarson O, Johnson M and Lundqvist B I 1979 *Phys. Rev.* B **20** 3136
[26] Jensen K O and Walker A B 1988 *J. Phys. F: Met. Phys.* **18** L277
[27] Nieminen R M and Puska M J 1983 *Phys. Rev. Lett.* **50** 281
[28] Nieminen R M, Puska M J and Maninnen M 1984 *Phys. Rev. Lett.* **53** 1298
[29] Daniuk S, Sob M and Rubaszek A 1991 *Phys. Rev.* B **43** 2580
[30] Kontrym-Sznajd G and Rubaszek A 1993 *Phys. Rev.* B **47** 6950
[31] Daniuk S 1989 *J. Phys.: Condens. Matter* **1** 5561
[32] Daniuk S, Kontrym-Sznajd G, Rubaszek A, Stachowiak H, Mayers J, Walters P A and West R N 1987 *J. Phys. F: Met. Phys.* **17** 1365
[33] Kiejna A 1991 *Phys. Rev.* B **43** 14 695
[34] Carbotte J P 1967 *Phys. Rev.* **155** 197
[35] Carbotte J P 1983 *Positron Solid State Physics* ed W Brandt and A Dupasquier (Amsterdam: North-Holland) p 32
[36] Stachowiak H and Rubaszek A 1993 *Positrons at Metallic Surfaces (Solid State Phenomena 28/29)* ed A Ishii (Aedermannsdorf: Trans. Tech.) p 7
[37] Hohenberg P and Kohn W 1964 *Phys. Rev.* **136** B864
[38] Kohn W and Sham L J 1965 *Phys. Rev.* **140** A1133
[39] Boev O V, Puska M J and Nieminen R M 1987 *Phys. Rev.* B **36** 7786
[40] Farjam M and Schroe H 1987 *Phys. Rev.* B **36** 5089
[41] Fletcher G, Fry J L and Pattnaik P C 1983 *Phys. Rev.* B **27** 3987
[42] Monnier R and Perdew J P 1978 *Phys. Rev.* B **17** 2595
[43] Serena P A, Soler J M and Garcia N 1986 *Phys. Rev.* B **34** 6767
[44] Ceperley D M and Alder B J 1980 *Phys. Rev. Lett.* **45** 566
[45] Perdew J P and Zunger A 1981 *Phys. Rev.* B **23** 5048
[46] Brandt W and Reinheimer J 1971 *Phys. Lett.* A **35** 109
[47] Liberman D A, Cromer D T and Waber J T 1971 *Comput. Phys. Commun* **2** 107
[48] Hedin L and Lundqvist B I 1971 *J. Phys. C: Solid State Phys.* **4** 2064
[49] Papaconstantopoulos D A 1986 *Handbook of the Band Structure of Elemental Solids* (New York: Plenum)
[50] Anderson O K, Jepsen O and Glötzel D 1985 *Highlights of Condensed Matter Theory* ed F Bassani, F Fumi and M P Tosi (Amsterdam: North-Holland)
[51] Mattheiss L F 1969 *Phys. Rev.* **134** A970
[52] Boroński E and Nieminen R M 1986 *Phys. Rev.* B **34** 3820
[53] *Handbook of Chemistry and Physics* 1986 67th edn (Boca Raton, FL: Chemical Rubber Company) p E-89
[54] Skriver H C 1984 *The LMTO Method* (New York: Springer)
[55] Moruzzi V L, Janak J F and Williams A R 1978 *Calculated Electronic Properties of Metals* (New York: Pergamon)
[56] Kontrym-Sznajd G and Daniuk S 1992 *Positron Annihilation (Mater. Sci. Forum 105–110)* ed Zs Kajcsos and Cs Szeles (Aedermannsdorf: Trans. Tech.) p 695
[57] Daniuk S, Kontrym-Sznajd G, Majsnerowski J, Stachowaik H and Šob M 1989 *J. Phys.: Condens. Matter* **1** 6321